



# Numerical Heat Transfer, Part A: Applications

## An International Journal of Computation and Methodology

ISSN: 1040-7782 (Print) 1521-0634 (Online) Journal homepage: <https://www.tandfonline.com/loi/unht20>

## Integral transform analysis of convective heat transfer within wavy walls channels

Helder K. Miyagawa, João N. N. Quaresma, Kleber M. Lisboa & Renato M. Cotta

To cite this article: Helder K. Miyagawa, João N. N. Quaresma, Kleber M. Lisboa & Renato M. Cotta (2020) Integral transform analysis of convective heat transfer within wavy walls channels, Numerical Heat Transfer, Part A: Applications, 77:5, 460-481, DOI: [10.1080/10407782.2020.1713619](https://doi.org/10.1080/10407782.2020.1713619)

To link to this article: <https://doi.org/10.1080/10407782.2020.1713619>



Published online: 04 Feb 2020.



Submit your article to this journal [↗](#)



Article views: 72







View related articles [↗](#)



View Crossmark data [↗](#)



# Integral transform analysis of convective heat transfer within wavy walls channels

Helder K. Miyagawa<sup>a</sup> , João N. N. Quaresma<sup>a</sup> , Kleber M. Lisboa<sup>b,c</sup> , and Renato M. Cotta<sup>c,d</sup> 

<sup>a</sup>School of Chemical Engineering and Graduate Program in Natural Resource Engineering in the Amazon, Institute of Technology, Federal University of Pará, UFPA, Campus Universitário do Guamá, Belém, Brazil; <sup>b</sup>Mechanical Engineering Department, Centro Federal de Educação Tecnológica Celso Suckow da Fonseca, CEFET/RJ, Rio de Janeiro, Brazil; <sup>c</sup>Mechanical Engineering Department, POLI & COPPE, Federal University of Rio de Janeiro, UFRJ, Brazil; <sup>d</sup>General Directorate of Nuclear and Technological Development, DGDNTM, Brazilian Navy, Rio de Janeiro, Brazil

## ABSTRACT

The generalized integral transform technique (GITT) is employed in the hybrid numerical-analytical solution of the two-dimensional Navier–Stokes and energy equations in wavy walls channels. The flow is considered laminar and incompressible for a Newtonian fluid with temperature-independent physical properties, while the walls temperatures are kept uniform along the channel length. The streamfunction-only formulation is adopted, which eliminates the pressure field and automatically satisfies the continuity equation. A thorough convergence analysis is performed for the streamfunction field, temperature field, friction factor, and local Nusselt number to illustrate the method robustness. The verification of the present GITT results is also performed by comparing the centerline velocity, friction factor, average temperature, and local Nusselt number with equivalent results from the COMSOL Multiphysics simulation platform, with overall very good agreement. The influence of the governing parameters such as Reynolds number and wavy-wall amplitude on the velocity and temperature fields is also analyzed, demonstrating their importance in the convective heat transfer behavior.

## ARTICLE HISTORY



Received 20 September 2019

Accepted 26 December 2019

## 1. Introduction

Heat transfer enhancement is a crucial factor in industrial processes that are intensive in thermal energy usage, while low fabrication cost, passive operation, and compact design are essential characteristics demanded from heat exchangers in such applications. Despite the increase in pressure drop in comparison with parallel plates passages in compact heat exchangers, wavy channels have been frequently considered as an alternative design toward heat transfer augmentation. Furthermore, there are biological applications, such as kidney dialyzers and membrane oxygenators, which involve the flow of a high viscosity fluid that remains in laminar regime along the usually narrow wavy channels, in light of the fairly low Reynolds number condition [1].

Heat and fluid flow in wavy walls channels was the focus of investigation in various previous studies on heat or mass transfer applications. Early experimental studies demonstrated the

**CONTACT** João N. N. Quaresma  [quaresma@ufpa.br](mailto:quaresma@ufpa.br)  School of Chemical Engineering and Graduate Program in Natural Resource Engineering in the Amazon, Institute of Technology, Federal University of Pará, UFPA, Campus Universitário do Guamá, Belém, Pará, Brazil.

Color versions of one or more of the figures in the article can be found online at [www.tandfonline.com/unht](http://www.tandfonline.com/unht).



For the arc-shaped configuration, the SIMPLE scheme (semi-implicit method for pressure-linked equations) of the finite volume method was applied, demonstrating that the recirculation is amplified with increasing Reynolds number, while an increase on the geometric parameters (channel height and wavelength) decreases the recirculation zone extent [11, 12]. Trapezoidal walls channels were also studied for a nanofluid flow, considering different geometrical parameters [13]. The results show that the Nusselt number increases with the nanoparticles fraction, the Reynolds number, and the amplitude of the channel. In microchannels with wavy walls [14], at  $Re = 200$ , it was reported that heat transfer was increased by 130%, whereas the friction factor increased by 35%. Again, for microchannels and water flow [15], it has been observed, for  $Re = 300$  and 400, that the heat transfer enhancement could be achieved without significant penalty on the pressure loss. Also, for an MHD (magnetohydrodynamics) situation [16], forced convection and entropy generation were investigated for a water- $Al_2O_3$  nanofluid flow in a sinusoidal wavy channel. It was demonstrated that increasing the applied magnetic field enhances the Nusselt number, while adding more nanoparticles increases the Nusselt number, but also increases the total entropy generation [16]. Heat transfer enhancement analyses involving the flow of nanofluids were also considered in different irregular geometric configurations [17–21], including the channel flow in turbulent regime [22, 23], and the entropy generation analysis in MHD plane diffuser [24].

Usually, solutions to complex heat and fluid flow problems are obtained by purely numerical methods. On the other hand, the GITT methodology [25–27] offers an interesting alternative hybrid numerical-analytical tool, based on eigenfunction expansions such as in the classical integral transform method. Such hybrid approach was successfully applied to various heat and fluid flow problems governed by either the boundary layer or the Navier–Stokes equations. Particularly in flow problems governed by the Navier–Stokes equations, there has been a preference to employ the streamfunction-only formulation instead of the primitive variables one, in two-dimensional models, due to the convenience of automatically eliminating the pressure field and satisfying the continuity equation. For instance, using the streamfunction-only formulation, some classical test problems have been analyzed, such as the lid-driven cavity flow [28], straight channel flow [29], the irregular gradual expansion channel [30], and MHD flow and heat transfer in parallel plates channel [31]. More recently, a new vector eigenfunction expansion concept was introduced for the GITT solution of the Navier–Stokes equations [32–35], aiming at extending the advantages of the streamfunction formulation to more general flow problems. The different possibilities of dealing with the Navier–Stokes equations under the GITT framework have been recently reviewed [36] and illustrated with representative examples. With respect to the flow problem in wavy channels, the GITT under the streamfunction formulation has already been considered for a sinusoidal profile and Reynolds number in the range of 100 to 500 [37]. Though good agreement was obtained in comparison with previous numerical studies [5], it has been more recently observed that both implementations [5, 37] could have been affected by numerical inconsistencies introduced by the domain derivatives singularities at the junctions of the wavy and straight sections [10]. The GITT was also applied to obtain an approximate solution for heat transfer in a wavy channel [38], later on including conjugation effects [39], but these simulations were performed for low enough Reynolds numbers to allow for employing an approximate velocity field based on a longitudinally variable polynomial profile that essentially satisfies the continuity equation.

The objective of the present work is to apply the GITT in solving both the Navier–Stokes and energy equations for a wavy wall channel geometry. The streamfunction formulation is once more preferred, with its inherent advantages for the proposed two-dimensional problem. The solution verification is accomplished by comparing the results for the velocity and temperature fields with those from the well-known COMSOL Multiphysics finite-elements-based commercial platform. Relevant local quantities such as the product of the friction factor by the Reynolds

number ( $fRe$ ) and the local Nusselt number ( $Nu_x$ ) are also computed and shown as functions of the longitudinal coordinate along the channel length. Then, the influence of the main governing parameters such as the Reynolds number ( $Re$ ) and the wavy wall amplitude ( $\alpha$ ) is quantified in terms of their importance to the heat transfer enhancement.

## 2. Mathematical formulation

The problem is defined by considering heat and fluid flow in steady state within a wavy walls channel, with two parallel plates at the beginning and at the end of the wavy duct. The fluid is considered to be Newtonian and the flow is assumed to be laminar and incompressible, subjected to a uniform temperature along the walls. Figure 1 shows the main characteristics of the geometry, coordinates system, and the boundary conditions.

### 2.1. Problem formulation

The continuity, Navier–Stokes, and energy equations for the analyzed problem, in dimensionless form, are written as:

$$\frac{\partial u}{\partial x} + \frac{\partial v}{\partial y} = 0, \quad (1a)$$

$$u \frac{\partial u}{\partial x} + v \frac{\partial u}{\partial y} = -\frac{\partial p}{\partial x} + \frac{1}{Re} \left( \frac{\partial^2 u}{\partial x^2} + \frac{\partial^2 u}{\partial y^2} \right), \quad (1b)$$

$$u \frac{\partial v}{\partial x} + v \frac{\partial v}{\partial y} = -\frac{\partial p}{\partial y} + \frac{1}{Re} \left( \frac{\partial^2 v}{\partial x^2} + \frac{\partial^2 v}{\partial y^2} \right), \quad (1c)$$

$$u \frac{\partial T}{\partial x} + v \frac{\partial T}{\partial y} = \frac{1}{RePr} \left( \frac{\partial^2 T}{\partial x^2} + \frac{\partial^2 T}{\partial y^2} \right), \quad -y_1 < y < y_2, \quad x > 0 \quad (1d)$$

These equations are subjected to the following boundary conditions (inlet, outlet, and walls):

$$x = 0 : \begin{cases} u = u_1(y) \\ v = v_1(y) \\ T = 1 \end{cases} ; \quad x = x_{out} : \begin{cases} \frac{\partial \omega}{\partial x} = 0 \\ v = 0 \\ \frac{\partial T}{\partial x} = 0 \end{cases} ; \quad y = -y_1 : \begin{cases} u = 0 \\ v = 0 \\ T = 0 \end{cases} ; \quad y = y_2 : \begin{cases} u = 0 \\ v = 0 \\ T = 0 \end{cases} \quad (1e-p)$$

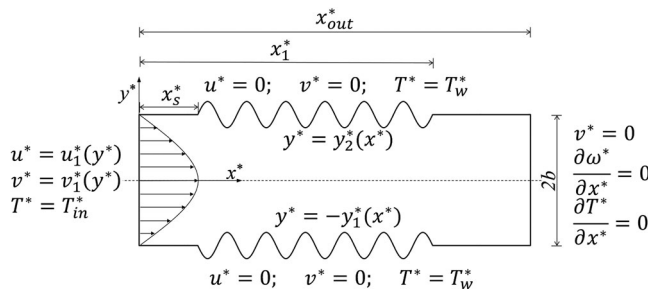


Figure 1. Geometric configuration and boundary conditions for the wavy walls channel.

The dimensionless groups here considered are:

$$\begin{aligned}
 x &= \frac{x^*}{b}; y = \frac{y^*}{b}; u = \frac{u^*}{u_{av}}; v = \frac{v^*}{u_{av}}; p = \frac{p^*}{\rho u_{av}^2}; T = \frac{T^* - T_w^*}{T_{in}^* - T_w^*}; \psi = \frac{\psi^*}{u_{av} b}; \omega = \frac{\omega^* b}{u_{av}}; x_{out} = \frac{x_{out}^*}{b}; \\
 y_1(x) &= \frac{y_1^*(x^*)}{b}; y_2(x) = \frac{y_2^*(x^*)}{b}; u_1(y) = \frac{u_1^*(y^*)}{u_{av}}; v_1(y) = \frac{v_1^*(y^*)}{u_{av}}; Re = \frac{u_{av} b}{\nu}; Pr = \frac{\nu}{\alpha}
 \end{aligned}
 \tag{2}$$

Here,  $y_1$  and  $y_2$  are the functions that describe the channel walls positions, which were the same as already studied in Refs. [5, 37], and are given as:

$$y_2(x) = y_1(x) = \begin{cases} 1, & \text{for } 0 \leq x \leq x_s \\ 1 + \alpha \sin[\pi(x - x_s)], & \text{for } x_s \leq x \leq x_l \\ 1, & \text{for } x_l \leq x \leq x_{out} \end{cases}
 \tag{3}$$

where  $\alpha=a/b$  is the dimensionless wavy-wall amplitude,  $x_s=x_s^*/b$  and  $x_l=x_l^*/b$  are the dimensionless positions for the beginning and the end of the wavy walls, respectively, and  $x_{out}=x_{out}^*/b$  is the dimensionless channel length.

To avoid numerical inconsistencies caused by the singularities introduced by the derivatives of the domain function defined in Eq. (3) [10], a continuous function is introduced to smooth the transition between the straight and sinusoidal sections of the channel depicted in Figure 1. The modified geometry is then given by:

$$y_2(x) = y_1(x) = 1 + \alpha \sin[\pi(x - x_s)][U_s(x, x_s) - U_s(x, x_l)]
 \tag{4}$$

where  $U_s(x, x')$  is a continuous approximation of the unit step function, which is given as

$$U_s(x, x') = \frac{1}{1 + \exp[-\beta(x - x')]}
 \tag{5}$$

where in Eq. (5),  $\beta$  is an adjustable parameter.

### 2.2. Streamfunction-only formulation

The streamfunction-only formulation is adopted, which results in the elimination of the pressure field, avoiding any further treatment of this dependent variable. Furthermore, the streamfunction formulation automatically satisfies the mass conservation law (continuity equation) and allows for a more straightforward visualization of the recirculation zones due to its intrinsic relation with the streamlines. Thus, the streamfunction definition is considered:

$$u = \frac{\partial \psi}{\partial y}; \quad v = -\frac{\partial \psi}{\partial x}
 \tag{6a,b}$$

To obtain the streamfunction-only formulation and to eliminate the pressure field, we take the derivative of Eqs. (1b) and (1c) with respect to the  $y$  and  $x$  variables, respectively, the results are subtracted and the definition of streamfunction given by Eqs. (6a) and (6b) is used in place of  $u$  and  $v$  velocity components, respectively. Also, with this streamfunction definition, the continuity equation given by Eq. (1a) is automatically satisfied. Therefore, the momentum and energy equations subjected to boundary conditions given by Eqs. (1e)–(1p) are rewritten as:

$$\frac{\partial \psi}{\partial y} \frac{\partial}{\partial x} (\nabla^2 \psi) - \frac{\partial \psi}{\partial x} \frac{\partial}{\partial y} (\nabla^2 \psi) = \frac{1}{Re} \nabla^4 \psi,
 \tag{7a}$$

$$\frac{\partial \psi}{\partial y} \frac{\partial T}{\partial x} - \frac{\partial \psi}{\partial x} \frac{\partial T}{\partial y} = \frac{1}{RePr} \left( \frac{\partial^2 T}{\partial x^2} + \frac{\partial^2 T}{\partial y^2} \right), \quad -y_1 < y < y_2, \quad x > 0
 \tag{7b}$$

where,  $\nabla^4$  is the biharmonic operator.

These equations are subjected to the boundary conditions:

$$x = 0 : \begin{cases} \psi = k_1 + \int_{-y_1}^y u_1(\eta) d\eta \\ \frac{\partial \psi}{\partial x} = -v_1(y) \\ T = 1 \end{cases} ; x = x_{out} : \begin{cases} \frac{\partial \psi}{\partial x} = 0 \\ \frac{\partial^3 \psi}{\partial x^3} + \frac{\partial^3 \psi}{\partial x \partial y^2} = 0 \\ \frac{\partial T}{\partial x} = 0 \end{cases} ; y = -y_1 : \begin{cases} \psi = k_1 \\ \frac{\partial \psi}{\partial \mathbf{n}} = 0 \\ T = 0 \end{cases} ; y = y_2 : \begin{cases} \psi = k_2 \\ \frac{\partial \psi}{\partial \mathbf{n}} = 0 \\ T = 0 \end{cases} \quad (7c-n)$$

The boundary conditions given by Eqs. (7c) and (7d), (7f) and (7g), (7i) and (7j), and (7l) and (7m) were also obtained applying the streamfunction definition given by Eqs. (6) on Eqs. (1e)–(1p) in place of the velocity components and in the vorticity definition. Also, some appropriate integrations were performed as in the case of Eqs. (7c), (7i), and (7l).

### 3. Solution methodology

#### 3.1. Filter solution

An analytical filter solution is employed to remove the nonhomogeneities of the boundary conditions in the transversal coordinate,  $y$ . This filtering leads to a marked improvement in the convergence rate of the streamfunction field,  $\psi(x,y)$ , by decreasing the importance of the boundary source terms [25, 26]. The relation between the streamfunction and its filter and filtered counterparts is given by:

$$\psi(x, y) = F(x, y) + \phi(x, y) \quad (8)$$

Here,  $F(x,y)$  is an adaptive filter that varies along the wavy surface length. The applied filter is not a particular solution of the full problem, but has the same values of the original potential at the walls of the channel [30, 37], and is given by:

$$F(x, y) = F(\xi) = \frac{3Q}{4} \left( \xi - \frac{\xi^3}{3} \right) + \frac{Q}{2} + k_1 \quad (9)$$

where,

$$\xi = \frac{y - y_3(x)}{y_0(x)} ; y_0(x) = \frac{y_2(x) + y_1(x)}{2} ; y_3(x) = \frac{y_2(x) - y_1(x)}{2} \quad (10a-c)$$

By applying these definitions into Eqs. (7), it results:

$$\begin{aligned} & \frac{\partial \phi}{\partial y} \frac{\partial^3 \phi}{\partial x^3} + \frac{\partial \phi}{\partial y} \frac{\partial^3 \phi}{\partial x \partial y^2} - \frac{\partial \phi}{\partial x} \frac{\partial^3 \phi}{\partial x^2 \partial y} - \frac{\partial \phi}{\partial x} \frac{\partial^3 \phi}{\partial y^3} + \frac{\partial \phi}{\partial y} \frac{\partial^3 F}{\partial x^3} + \frac{\partial \phi}{\partial y} \frac{\partial^3 F}{\partial x \partial y^2} - \frac{\partial \phi}{\partial x} \frac{\partial^3 F}{\partial x^2 \partial y} - \frac{\partial \phi}{\partial x} \frac{\partial^3 F}{\partial y^3} + \\ & \frac{\partial F}{\partial y} \frac{\partial^3 \phi}{\partial x^3} + \frac{\partial F}{\partial y} \frac{\partial^3 \phi}{\partial x \partial y^2} - \frac{\partial F}{\partial x} \frac{\partial^3 \phi}{\partial x^2 \partial y} - \frac{\partial F}{\partial x} \frac{\partial^3 \phi}{\partial y^3} + \frac{\partial F}{\partial y} \frac{\partial^3 F}{\partial x^3} + \frac{\partial F}{\partial y} \frac{\partial^3 F}{\partial x \partial y^2} - \frac{\partial F}{\partial x} \frac{\partial^3 F}{\partial x^2 \partial y} - \frac{\partial F}{\partial x} \frac{\partial^3 F}{\partial y^3} \\ & = \frac{1}{Re} \left( \frac{\partial^4 \phi}{\partial x^4} + 2 \frac{\partial^4 \phi}{\partial x^2 \partial y^2} + \frac{\partial^4 \phi}{\partial y^4} + \frac{\partial^4 F}{\partial x^4} + 2 \frac{\partial^4 F}{\partial x^2 \partial y^2} \right) \end{aligned} \quad (11a)$$

$$\frac{\partial \phi}{\partial y} \frac{\partial T}{\partial x} - \frac{\partial \phi}{\partial x} \frac{\partial T}{\partial y} + \frac{\partial F}{\partial y} \frac{\partial T}{\partial x} - \frac{\partial F}{\partial x} \frac{\partial T}{\partial y} = \frac{1}{RePr} \left( \frac{\partial^2 T}{\partial x^2} + \frac{\partial^2 T}{\partial y^2} \right), \quad -y_1 < y < y_2, \quad x > 0 \quad (11b)$$

$$x = 0 : \begin{cases} \phi = k_1 + \int_{-y_1}^y u_1(\eta) d\eta - F \\ \frac{\partial \phi}{\partial x} = -v_1(y) - \frac{\partial F}{\partial x} \\ T = 1 \end{cases} ; x = x_{out} : \begin{cases} \frac{\partial \phi}{\partial x} = -\frac{\partial F}{\partial x} \\ \frac{\partial^3 \phi}{\partial x^3} + \frac{\partial^3 \phi}{\partial x \partial y^2} = -\left(\frac{\partial^3 F}{\partial x^3} + \frac{\partial^3 F}{\partial x \partial y^2}\right) \\ \frac{\partial T}{\partial x} = 0 \end{cases} \quad (11c-h)$$

$$y = -y_1 : \begin{cases} \phi = 0 \\ \frac{\partial \phi}{\partial \mathbf{n}} = 0 \\ T = 0 \end{cases} ; y = y_2 : \begin{cases} \phi = 0 \\ \frac{\partial \phi}{\partial \mathbf{n}} = 0 \\ T = 0 \end{cases} \quad (11i-n)$$

The constants  $k_1$  and  $k_2$  represent the values of the streamfunction at the duct walls, and can be computed applying the relationship between the streamfunction and the longitudinal velocity at the beginning of the channel given by Eq. (7c) and evaluating it at  $y = y_2$ , yielding:

$$k_2 = k_1 + Q \quad (12)$$

The values of  $k_1$  and  $k_2$  can be specified as  $-1$  and  $1$ , respectively, and, to satisfy Eq. (12), it results in  $Q = 2$ . It is important to note that the boundary conditions given by Eqs. (1d) and (1e) represent a general form of the longitudinal and transversal velocity components, respectively. However, in the present study, we adopt the special case of parallel flow with a parabolic distribution for  $u_1(y)$  at the channel entry, leading to:

$$u_1(y) = 3(1 - y^2)/2; v_1(y) = 0 \quad (13a,b)$$

### 3.2. Integral transformation

The integral transformation of Eqs. (11), after the homogenization of the wall boundary conditions, is now performed. The first step is to choose the eigenvalue problems for the streamfunction and temperature distributions.

- For the streamfunction field the following fourth order eigenvalue problem was chosen:

$$\frac{\partial^4 Y_i(x, y)}{\partial y^4} = \mu_i^4 Y_i(x, y), \quad -y_1 < y < y_2 \quad (14a)$$

$$Y_i(x, -y_1) = 0; \frac{\partial Y_i(x, -y_1)}{\partial \mathbf{n}} = 0; Y_i(x, y_2) = 0; \frac{\partial Y_i(x, y_2)}{\partial \mathbf{n}} = 0 \quad (14b-e)$$

or in terms of the redefined transversal coordinate,  $\xi$ , given in Eq. (10a):

$$\frac{d^4 Y_i(\xi)}{d\xi^4} = \beta_i^4 Y_i(\xi), \quad -1 < \xi < 1 \quad (14f)$$

$$Y_i(-1) = 0; \frac{dY_i(-1)}{d\xi} = 0; Y_i(1) = 0; \frac{dY_i(1)}{d\xi} = 0 \quad (14g-j)$$

where the relationship  $\beta_i = \mu_i y_0$  applies, and  $y_0$  was defined in Eq. (10b). The eigenvalue problem in terms of the  $\xi$ -coordinate has the following analytical solution:



$$Y_i(\xi) = \begin{cases} \frac{\cos(\beta_i \xi)}{\cos(\beta_i)} - \frac{\cosh(\beta_i \xi)}{\cosh(\beta_i)}, & i = 1, 3, 5, \dots \\ \frac{\sin(\beta_i \xi)}{\sin(\beta_i)} - \frac{\sinh(\beta_i \xi)}{\sinh(\beta_i)}, & i = 2, 4, 6, \dots \end{cases} \quad (14k)$$

The eigenvalues  $\beta_i$  can be calculated from the following nonlinear algebraic equations:

$$\tan(\beta_i) = \begin{cases} -\tanh(\beta_i), & i = 1, 3, 5, \dots \\ \tanh(\beta_i), & i = 2, 4, 6, \dots \end{cases} \quad (14l)$$

The eigenfunctions  $Y_i(x, y)$  have the following orthogonality property:

$$\int_{-y_1}^{y_2} Y_i(x, y) Y_j(x, y) dy = \begin{cases} 0, & i \neq j \\ 2y_0(x) = M_i, & i = j \end{cases} \quad (14m)$$

where  $M_i$  is the normalization integral.

The eigenvalue problem given by Eqs. (14) allows for the definition of the following integral-transform pair:

$$\bar{\phi}_i(x) = \frac{1}{M_i} \int_{-y_1}^{y_2} Y_i(x, y) \phi(x, y) dy, \quad \text{transform} \quad (15a)$$

$$\phi(x, y) = \sum_{i=1}^{\infty} Y_i(x, y) \bar{\phi}_i(x), \quad \text{inverse} \quad (15b)$$

- For the temperature field, the chosen eigenvalue problem is written as:

$$\frac{\partial^2 \Gamma_i(x, y)}{\partial y^2} = -\lambda_i^2 \Gamma_i(x, y), \quad -y_1 < y < y_2 \quad (16a)$$

$$\Gamma_i(x, -y_1) = 0; \quad \Gamma_i(x, y_2) = 0 \quad (16b, c)$$

In terms of the redefined independent variable,  $\xi$ :

$$\frac{d^2 \Gamma_i(\xi)}{d\xi^2} = -\gamma_i^2 \Gamma_i(\xi), \quad -1 < \xi < 1 \quad (16d)$$

$$\Gamma_i(-1) = 0; \quad \Gamma_i(1) = 0 \quad (16e, f)$$

The eigenfunctions, eigenvalues and the normalization integral are analytically obtained as:

$$\Gamma_i(\xi) = \sin[\gamma_i(\xi + 1)]; \quad \gamma_i = \frac{i\pi}{2}; \quad \lambda_i = \frac{\gamma_i}{y_0(x)}, \quad i = 1, 2, 3, \dots \quad (16g-i)$$

$$\int_{-y_1}^{y_2} \Gamma_i(x, y) \Gamma_j(x, y) dy = \begin{cases} 0, & i \neq j \\ y_0(x) = N_i, & i = j \end{cases} \quad (16j)$$

Therefore, the integral-transform pair for the temperature field is then defined as:

$$\bar{T}_i(x) = \frac{1}{N_i} \int_{-y_1}^{y_2} \Gamma_i(x, y) T(x, y) dy, \quad \text{transform} \quad (17a)$$

$$T(x, y) = \sum_{i=1}^{\infty} \Gamma_i(x, y) \bar{T}_i(x), \quad \text{inverse} \quad (17b)$$

Finally, the problem defined by Eqs. (11) is now integral transformed. For this purpose, Eq. (11a) is multiplied by  $Y_i(x, y)$  and Eq. (11b) by  $\Gamma_i(x, y)$ , respectively, and then, integrated across the domain  $[-y_1, y_2]$  in the  $y$ -direction. The eigenfunctions orthogonality properties are then used

in conjunction with the inverse formulae given by Eqs. (15b) and (17b) to furnish the following coupled system of ordinary differential equations in the  $x$ -direction:

$$\begin{aligned} \frac{d^4 \bar{\phi}_i(x)}{dx^4} &= -\mu_i^4 \bar{\phi}_i + \frac{A_i}{M_i} + \frac{1}{M_i} \sum_{j=1}^{\infty} \left\{ B_{ij} \bar{\phi}_j + C_{ij} \bar{\phi}'_j + D_{ij} \bar{\phi}''_j + E_{ij} \bar{\phi}'''_j \right\} \\ &+ \frac{Re}{M_i} \sum_{i=1}^{\infty} \sum_{j=1}^{\infty} \left\{ F_{ijk} \bar{\phi}_j \bar{\phi}_k + G_{ijk} \bar{\phi}_j \bar{\phi}'_k + H_{ijk} \bar{\phi}_j \bar{\phi}''_k + I_{ijk} \bar{\phi}_j \bar{\phi}'''_k + J_{ijk} \bar{\phi}'_j \bar{\phi}_k + K_{ijk} \bar{\phi}'_j \bar{\phi}'_k + L_{ijk} \bar{\phi}'_j \bar{\phi}''_k \right\} \end{aligned} \tag{18a}$$

$$\frac{d^2 \bar{T}_i(x)}{dx^2} = \lambda_i^2 \bar{T}_i + \frac{1}{N_i} \sum_{j=1}^{\infty} (O_{ij} \bar{T}_j + P_{ij} \bar{T}'_j) + \frac{RePr}{N_i} \sum_{j=1}^{\infty} \sum_{k=1}^{\infty} (Q_{ijk} \bar{T}'_j \bar{\phi}_k + R_{ijk} \bar{T}_j \bar{\phi}'_k) \tag{18b}$$

The boundary conditions in the  $x$ -direction are similarly integral transformed, to yield:

$$\bar{\phi}_i(0) = 0; \quad \frac{d\bar{\phi}_i(0)}{dx} = 0; \quad \bar{T}_i(0) = \bar{a}_i \tag{18c-e}$$

$$\frac{d\bar{\phi}_i(x_{out})}{dx} = \bar{b}_i + \sum_{j=1}^{\infty} \bar{c}_{ij} \bar{\phi}_j(x_{out}) \tag{18f}$$

$$\frac{d^3 \bar{\phi}_i(x_{out})}{dx^3} = \bar{d}_i + \sum_{j=1}^{\infty} \left[ \bar{e}_{ij} \bar{\phi}_j(x_{out}) + \bar{f}_{ij} \bar{\phi}'_j(x_{out}) + \bar{g}_{ij} \bar{\phi}''_j(x_{out}) \right] \tag{18g}$$

$$\frac{d\bar{T}_i(x_{out})}{dx} = \sum_{j=1}^{\infty} \bar{h}_{ij} \bar{T}_j(x_{out}) \tag{18h}$$

The coefficients resulting from the integral transformation process are analytically evaluated by symbolic computation, being functions of the  $x$ -direction, and thus have to be computed along the solution procedure of the system of ODEs. Therefore, they are defined as:

$$A_i = - \int_{-y_1}^{y_2} Y_i \left( \frac{\partial^4 F}{\partial x^4} + 2 \frac{\partial^4 F}{\partial x^2 \partial y^2} \right) dy + Re \int_{-y_1}^{y_2} Y_i \left( \frac{\partial F}{\partial y} \frac{\partial^3 F}{\partial x^3} + \frac{\partial F}{\partial y} \frac{\partial^3 F}{\partial x \partial y^2} - \frac{\partial F}{\partial x} \frac{\partial^3 F}{\partial x^2 \partial y} - \frac{\partial F}{\partial x} \frac{\partial^3 F}{\partial y^3} \right) dy \tag{19a}$$

$$\begin{aligned} B_{ij} &= - \int_{-y_1}^{y_2} Y_i \frac{\partial^4 Y_j}{\partial x^4} dy - 2 \int_{-y_1}^{y_2} Y_i \frac{\partial^4 Y_j}{\partial x^2 \partial y^2} dy + Re \left[ \int_{-y_1}^{y_2} Y_i \frac{\partial Y_j}{\partial y} \frac{\partial^3 F}{\partial x^3} dy + \int_{-y_1}^{y_2} Y_i \frac{\partial Y_j}{\partial y} \frac{\partial^3 F}{\partial x \partial y^2} dy \right. \\ &- \int_{-y_1}^{y_2} Y_i \frac{\partial Y_j}{\partial x} \frac{\partial^3 F}{\partial x^2 \partial y} dy - \int_{-y_1}^{y_2} Y_i \frac{\partial Y_j}{\partial x} \frac{\partial^3 F}{\partial y^3} dy + \int_{-y_1}^{y_2} Y_i \frac{\partial^3 Y_j}{\partial x^3} \frac{\partial F}{\partial y} dy + \int_{-y_1}^{y_2} Y_i \frac{\partial^3 Y_j}{\partial x \partial y^2} \frac{\partial F}{\partial y} dy \\ &\left. - \int_{-y_1}^{y_2} Y_i \frac{\partial^3 Y_j}{\partial x^2 \partial y} \frac{\partial F}{\partial x} dy - \int_{-y_1}^{y_2} Y_i \frac{\partial^3 Y_j}{\partial y^3} \frac{\partial F}{\partial x} dy \right] \end{aligned} \tag{19b}$$

$$\begin{aligned} C_{ij} &= -4 \int_{-y_1}^{y_2} Y_i \frac{\partial^3 Y_j}{\partial x^3} dy - 4 \int_{-y_1}^{y_2} Y_i \frac{\partial^3 Y_j}{\partial x \partial y^2} dy + Re \left[ - \int_{-y_1}^{y_2} Y_i Y_j \frac{\partial^3 F}{\partial x^2 \partial y} dy - \int_{-y_1}^{y_2} Y_i Y_j \frac{\partial^3 F}{\partial y^3} dy \right. \\ &\left. + 3 \int_{-y_1}^{y_2} Y_i \frac{\partial^2 Y_j}{\partial x^2} \frac{\partial F}{\partial y} dy + \int_{-y_1}^{y_2} Y_i \frac{\partial^2 Y_j}{\partial y^2} \frac{\partial F}{\partial y} dy - 2 \int_{-y_1}^{y_2} Y_i \frac{\partial^2 Y_j}{\partial x \partial y} \frac{\partial F}{\partial x} dy \right] \end{aligned} \tag{19c}$$

$$D_{ij} = -6 \int_{-y_1}^{y_2} Y_i \frac{\partial^2 Y_j}{\partial x^2} dy - 2 \int_{-y_1}^{y_2} Y_i \frac{\partial^2 Y_j}{\partial y^2} dy + Re \left[ 3 \int_{-y_1}^{y_2} Y_i \frac{\partial Y_j}{\partial x} \frac{\partial F}{\partial y} dy - \int_{-y_1}^{y_2} Y_i \frac{\partial Y_j}{\partial y} \frac{\partial F}{\partial x} dy \right] \quad (19d)$$

$$E_{ij} = -4 \int_{-y_1}^{y_2} Y_i \frac{\partial Y_j}{\partial x} dy + Re \int_{-y_1}^{y_2} Y_i Y_j \frac{\partial F}{\partial y} dy \quad (19e)$$

$$F_{ijk} = \int_{-y_1}^{y_2} Y_i \frac{\partial Y_j}{\partial y} \frac{\partial^3 Y_k}{\partial x^3} dy + \int_{-y_1}^{y_2} Y_i \frac{\partial Y_j}{\partial y} \frac{\partial^3 Y_k}{\partial x \partial y^2} dy - \int_{-y_1}^{y_2} Y_i \frac{\partial Y_j}{\partial x} \frac{\partial^3 Y_k}{\partial x^2 \partial y} dy - \int_{-y_1}^{y_2} Y_i \frac{\partial Y_j}{\partial x} \frac{\partial^3 Y_k}{\partial y^3} dy \quad (19f)$$

$$G_{ijk} = 3 \int_{-y_1}^{y_2} Y_i \frac{\partial Y_j}{\partial y} \frac{\partial^2 Y_k}{\partial x^2} dy + \int_{-y_1}^{y_2} Y_i \frac{\partial Y_j}{\partial y} \frac{\partial^2 Y_k}{\partial y^2} dy - 2 \int_{-y_1}^{y_2} Y_i \frac{\partial Y_j}{\partial x} \frac{\partial^2 Y_k}{\partial x \partial y} dy \quad (19g)$$

$$H_{ijk} = 3 \int_{-y_1}^{y_2} Y_i \frac{\partial Y_j}{\partial y} \frac{\partial Y_k}{\partial x} dy - \int_{-y_1}^{y_2} Y_i \frac{\partial Y_j}{\partial x} \frac{\partial Y_k}{\partial y} dy; I_{ijk} = \int_{-y_1}^{y_2} Y_i \frac{\partial Y_j}{\partial y} Y_k dy \quad (19h,i)$$

$$J_{ijk} = - \int_{-y_1}^{y_2} Y_i Y_j \frac{\partial^3 Y_k}{\partial x^2 \partial y} dy - \int_{-y_1}^{y_2} Y_i Y_j \frac{\partial^3 Y_k}{\partial y^3} dy; K_{ijk} = -2 \int_{-y_1}^{y_2} Y_i Y_j \frac{\partial^2 Y_k}{\partial x \partial y} dy; L_{ijk} = - \int_{-y_1}^{y_2} Y_i Y_j \frac{\partial Y_k}{\partial y} dy \quad (19j-l)$$

$$O_{ij} = - \int_{-y_1}^{y_2} \Gamma_i \frac{\partial^2 \Gamma_j}{\partial x^2} dy; P_{ij} = -2 \int_{-y_1}^{y_2} \Gamma_i \frac{\partial \Gamma_j}{\partial x} dy + RePr \int_{-y_1}^{y_2} \Gamma_i \Gamma_j \frac{\partial F}{\partial y} dy \quad (19m,n)$$

$$Q_{ijk} = \int_{-y_1}^{y_2} \Gamma_i \Gamma_j \frac{\partial Y_k}{\partial y} dy; R_{ijk} = \int_{-y_1}^{y_2} \Gamma_i \frac{\partial \Gamma_j}{\partial y} Y_k dy \quad (19o,p)$$

$$\bar{a}_i = \frac{1}{y_0(0)} \int_{-y_1(0)}^{y_2(0)} \Gamma_i(0, y) dy; \bar{b}_i = - \frac{1}{2y_0(x_{out})} \int_{-y_1(x_{out})}^{y_2(x_{out})} Y_i(x_{out}, y) \frac{\partial F(x_{out}, y)}{\partial x} dy \quad (19q,r)$$

$$\bar{c}_{ij} = - \frac{1}{2y_0(x_{out})} \int_{-y_1(x_{out})}^{y_2(x_{out})} Y_i(x_{out}, y) \frac{\partial Y_j(x_{out}, y)}{\partial x} dy \quad (19s)$$

$$\bar{d}_i = - \frac{1}{2y_0(x_{out})} \int_{-y_1(x_{out})}^{y_2(x_{out})} Y_i(x_{out}, y) \left[ \frac{\partial^3 F(x_{out}, y)}{\partial x^3} + \frac{\partial^3 F(x_{out}, y)}{\partial x \partial y^2} \right] dy \quad (19t)$$

$$\bar{e}_{ij} = - \frac{1}{2y_0(x_{out})} \int_{-y_1(x_{out})}^{y_2(x_{out})} Y_i(x_{out}, y) \left[ \frac{\partial^3 Y_j(x_{out}, y)}{\partial x^3} + \frac{\partial^3 Y_j(x_{out}, y)}{\partial x \partial y^2} \right] dy \quad (19u)$$

$$\bar{f}_{ij} = - \frac{1}{2y_0(x_{out})} \int_{-y_1(x_{out})}^{y_2(x_{out})} Y_i(x_{out}, y) \left[ 3 \frac{\partial^2 Y_j(x_{out}, y)}{\partial x^2} + \frac{\partial^2 Y_j(x_{out}, y)}{\partial y^2} \right] dy \quad (19v)$$

$$\bar{g}_{ij} = - \frac{3}{2y_0(x_{out})} \int_{-y_1(x_{out})}^{y_2(x_{out})} Y_i(x_{out}, y) \frac{\partial Y_j(x_{out}, y)}{\partial x} dy \quad (19w)$$

$$\bar{h}_{ij} = - \frac{1}{y_0(x_{out})} \int_{-y_1(x_{out})}^{y_2(x_{out})} \Gamma_i(x_{out}, y) \frac{\partial \Gamma_j(x_{out}, y)}{\partial x} dy \quad (19x)$$

### 3.3. Relevant quantities

For the heat and fluid flow analysis, a few relevant dimensionless quantities are here calculated. First, the shear stress at the wall surface is given by:

$$\tau_w = -\mu \left( \frac{\partial u^*}{\partial y^*} + \frac{\partial v^*}{\partial x^*} \right)_{y^*=y_2^*} \tag{21}$$

The friction factor coefficient is defined as:

$$f = \frac{\tau_w}{\rho u_{av}^2} \tag{22}$$

Using Eqs. (21) and (22) together with the definition of the streamfunction given by Eqs. (6), the product of the friction factor coefficient by the Reynolds number,  $fRe$ , can be calculated from:

$$fRe = - \left( \frac{\partial^2 \psi}{\partial y^2} - \frac{\partial^2 \psi}{\partial x^2} \right) \Big|_{y=y_2} \tag{23}$$

or, by applying the filtering scheme given by Eq. (8) and the inverse formula defined in Eq. (15b), it follows:

$$fRe = - \left[ \frac{\partial^2 F}{\partial y^2} \Big|_{y=y_2} - \frac{\partial^2 F}{\partial x^2} \Big|_{y=y_2} + \sum_{i=1}^{\infty} \left( \frac{\partial^2 Y_i}{\partial y^2} \Big|_{y=y_2} - \frac{\partial^2 Y_i}{\partial x^2} \Big|_{y=y_2} \right) \bar{\phi}_i(x) \right] \tag{24}$$

The local Nusselt number is defined by:

$$Nu_x = \frac{hb}{k} = - \frac{b}{(T_{av}^* - T_w^*)} \frac{\partial T^*}{\partial \mathbf{n}^*} \Big|_{y^*=y_2^*} \tag{25}$$

or in terms of the dimensionless variables:

$$Nu_x = \frac{1}{T_{av}} \sqrt{ \left[ \left( \frac{\partial T}{\partial x} \right)^2 + \left( \frac{\partial T}{\partial y} \right)^2 \right] \Big|_{y=y_2} } \tag{26}$$

The bulk temperature in dimensionless form is given as:

$$T_{av}(x) = \frac{\int_{-y_1}^{y_2} u(x,y) T(x,y) dy}{(k_2 - k_1)} \tag{27}$$

### 4. Results

The coupled infinite system of ordinary differential equations given by Eqs. (18) is truncated to a finite number of terms (more specifically, NV terms for the streamfunction field and NT terms for the temperature field). This transformed ODE system is numerically solved using the DBVFPD subroutine [40] with a relative error control of  $10^{-4}$ . This subroutine is suitable for solving ODE boundary value problems with stiff characteristics. The results, unless otherwise stated, were calculated using NV = 50 and NT = 100 terms to guarantee converged results for both fields. The coefficients defined in Eqs. (19) were analytically obtained using the symbolic manipulation software *Mathematica* [41]. The value  $Pr=6.93$  was adopted for the Prandtl number (typical of water) in all computations. Also, in this study we have taken  $x_{out}=20$ , except where indicated. In addition, the remaining lengths are taken as  $x_s = 3$  and  $x_l = 15$ , which comprises six complete sinusoidal waves in the wavy part of the channel.

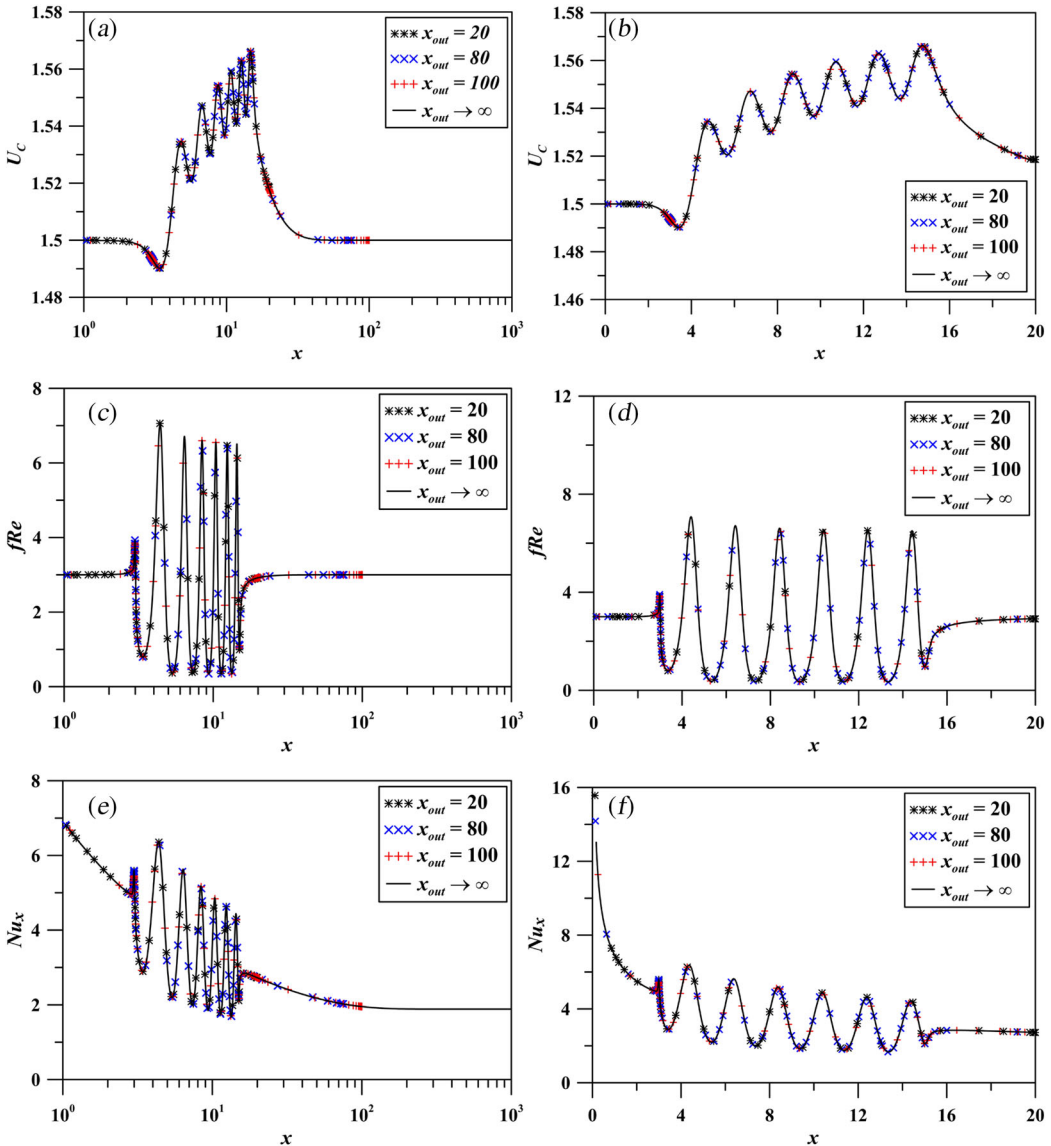


**Figure 2.** Comparison of the results for different values of  $x_{out}$  for  $Re = 100$  and  $\alpha = 0.1$ : (a) and (b) centerline velocity component; (c) and (d)  $fRe$  product; (e) and (f) local Nusselt number.

#### 4.1. Boundary conditions verification

It is important to mention that the present analysis is not limited to handling the channel with different truncated length  $x_{out}$ . Still, it can deal with the situation when  $x_{out} \rightarrow \infty$  and such integral transform analysis was considered in Pérez Guerrero et al. [30], where the outflow boundary conditions fully developed flow and temperature profiles are exactly recovered. Therefore, the outflow boundary conditions at  $x = x_{out}$  were firstly investigated to guarantee that the results obtained considering  $x_{out} = 20$  (or larger values), were the same as those obtained with  $x_{out} \rightarrow \infty$ . The studied case was  $Re = 100$  and  $\alpha = 0.1$ , with  $NV = 50$  and  $NT = 100$ .

Figures 2 represent the results considering  $Re = 100$  and  $\alpha = 0.1$  for various values of  $x_{out}$ , compared to results obtained by imposing the fully developed region at  $x_{out} \rightarrow \infty$ . Figures 2(a, c, e) provide results that extend to very large lengths while Figures 2(b, d, f) show just the length of the

truncated channel at  $x_{out} = 20$ . As can be observed, there is no significant difference among the results at the same axial positions for the centerline velocity component, product of the friction factor by the Reynolds number, and local Nusselt number for all  $x_{out}$  conditions, which indicates the adequacy of reducing the computational effort adopting a truncated channel with  $x_{out} = 20$ .

**4.2. Convergence analysis**

The convergence analysis for the streamfunction and temperature fields are illustrated by showing the computed values at  $y = 0.5$  and  $y = 1$ , respectively, for increasing truncation orders, while the friction factor and the local Nusselt number convergence are demonstrated graphically.

Tables 1 and 2 illustrate the convergence behavior of the streamfunction for two cases,  $Re = 100$  and  $\alpha = 0.3$ , and  $Re = 500$  and  $\alpha = 0.1$ , respectively. The streamfunction convergence for

**Table 1.** Convergence behavior of streamfunction field in different axial positions for  $Re = 100$  and  $\alpha = 0.3$ .

$\psi(x, y = 0.5)$									
NV = NT	$x = 1.5$	$x = 3.5$	$x = 5.5$	$x = 7.5$	$x = 9.5$	$x = 11.5$	$x = 13.5$	$x = 15.5$	$x = 20$
10	0.6875	0.6886	0.8008	0.8105	0.8160	0.8190	0.8208	0.8123	0.7278
20	0.6875	0.6885	0.8031	0.8123	0.8176	0.8205	0.8223	0.8138	0.7283
30	0.6875	0.6884	0.8031	0.8123	0.8176	0.8206	0.8223	0.8138	0.7283
40	0.6875	0.6884	0.8031	0.8123	0.8176	0.8206	0.8223	0.8138	0.7283
50	0.6875	0.6883	0.8031	0.8123	0.8176	0.8206	0.8223	0.8138	0.7283

**Table 2.** Convergence behavior of streamfunction field in different axial positions for  $Re = 500$  and  $\alpha = 0.1$ .

$\psi(x, y = 0.5)$									
NV = NT	$x = 1.5$	$x = 3.5$	$x = 5.5$	$x = 7.5$	$x = 9.5$	$x = 11.5$	$x = 13.5$	$x = 15.5$	$x = 20$
10	0.6875	0.6852	0.6939	0.6974	0.6996	0.7012	0.7025	0.7036	0.6955
20	0.6875	0.6855	0.6980	0.7016	0.7039	0.7057	0.7070	0.7072	0.6969
30	0.6875	0.6855	0.6980	0.7017	0.7040	0.7058	0.7071	0.7073	0.6970
40	0.6875	0.6855	0.6980	0.7016	0.7040	0.7057	0.7071	0.7073	0.6970
50	0.6875	0.6855	0.6980	0.7016	0.7040	0.7057	0.7071	0.7073	0.6970

**Table 3.** Convergence behavior of temperature field in different axial positions for  $Re = 100$  and  $\alpha = 0.3$ .

$T(x, y = 1)$							
NV	NT	$x = 3.5$	$x = 5.5$	$x = 7.5$	$x = 9.5$	$x = 11.5$	$x = 13.5$
30	30	0.3495	0.2354	0.2103	0.1948	0.1831	0.1739
40	40	0.3497	0.2369	0.2116	0.1959	0.1841	0.1748
50	50	0.3498	0.2368	0.2114	0.1958	0.1840	0.1748
50	60	0.3498	0.2367	0.2114	0.1958	0.1840	0.1747
50	70	0.3498	0.2368	0.2115	0.1958	0.1840	0.1748
50	80	0.3498	0.2367	0.2114	0.1958	0.1840	0.1747
50	90	0.3498	0.2367	0.2114	0.1958	0.1840	0.1747

**Table 4.** Convergence behavior of temperature field in different axial positions for  $Re = 500$  and  $\alpha = 0.1$ .

$T(x, y = 1)$							
NV	NT	$x = 3.5$	$x = 5.5$	$x = 7.5$	$x = 9.5$	$x = 11.5$	$x = 13.5$
30	30	0.3766	0.2210	0.1985	0.1831	0.1720	0.1633
40	40	0.3783	0.2208	0.1978	0.1828	0.1717	0.1631
50	50	0.3787	0.2211	0.1980	0.1830	0.1720	0.1633
50	60	0.3784	0.2209	0.1979	0.1829	0.1719	0.1632
50	70	0.3783	0.2209	0.1979	0.1829	0.1718	0.1632
50	80	0.3783	0.2209	0.1979	0.1829	0.1719	0.1632
50	90	0.3783	0.2209	0.1979	0.1829	0.1719	0.1632

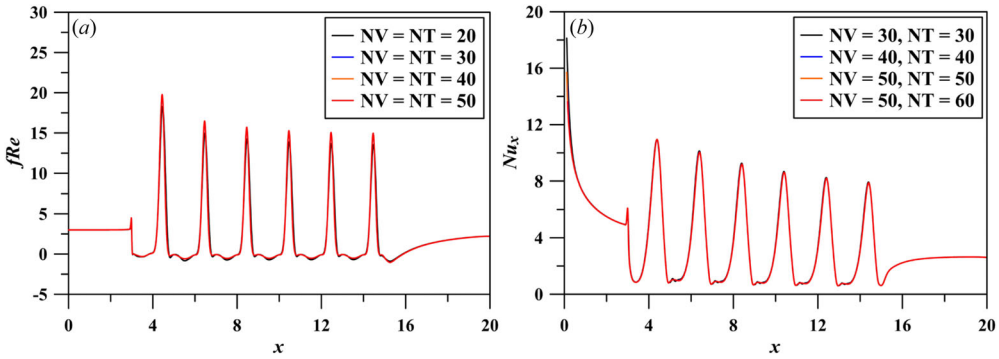


**Figure 3.** Convergence behavior of (a) friction-factor Reynolds number product and (b) local Nusselt number along the longitudinal coordinate for  $Re = 100$  and  $\alpha = 0.3$ .

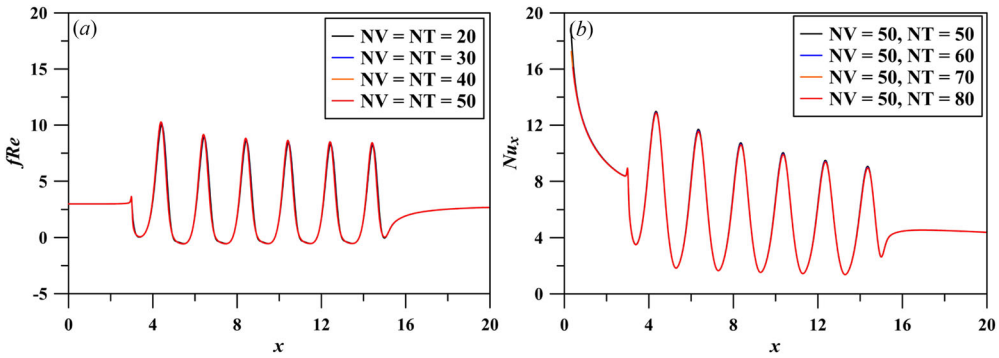


**Figure 4.** Convergence behavior of (a) friction-factor Reynolds number product and (b) local Nusselt number along the longitudinal coordinate for  $Re = 500$  and  $\alpha = 0.1$ .

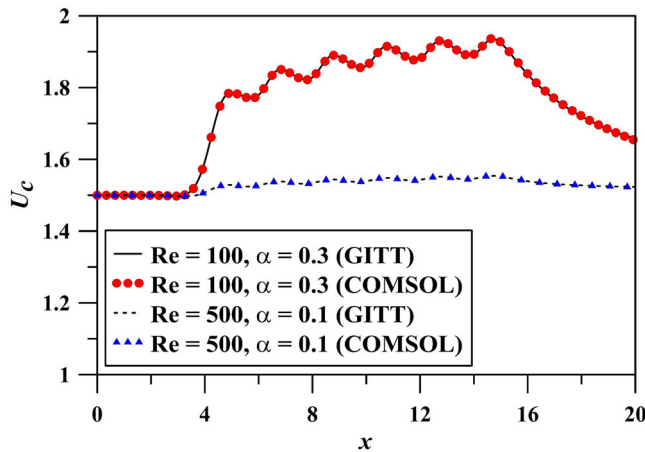


**Figure 5.** Comparisons of the central velocity component along the channel against COMSOL results.

both cases is very good, and the results are fully converged to the fourth significant digit (plus or minus one in the last digit shown) within 30 to 40 terms in all longitudinal positions considered (even with less terms in most positions).

Tables 3 and 4 illustrate the convergence behavior for the temperature field in the cases with  $Re = 100$  and  $\alpha = 0.3$ , and  $Re = 500$  and  $\alpha = 0.1$ , respectively. From Table 3, it is possible to

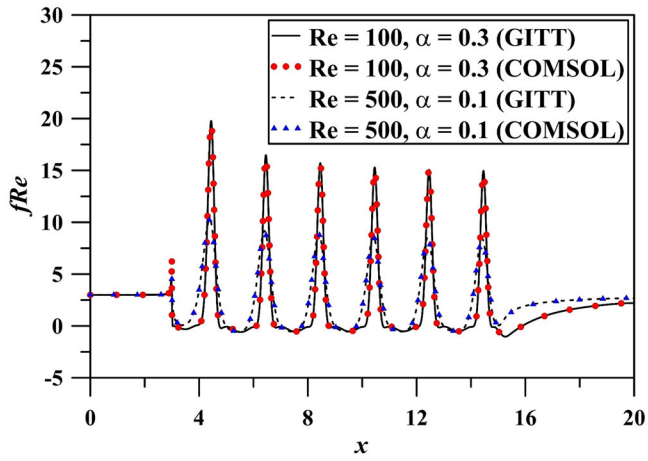


Figure 6. Comparisons of the  $fRe$  product along the channel against COMSOL results.

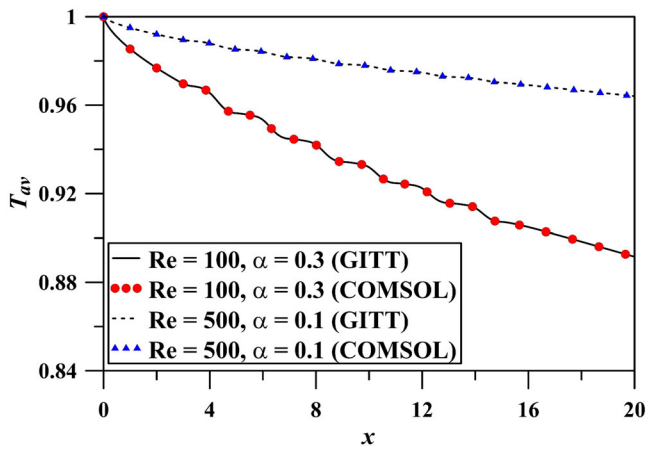


Figure 7. Comparisons of the bulk temperature along the channel against COMSOL results.

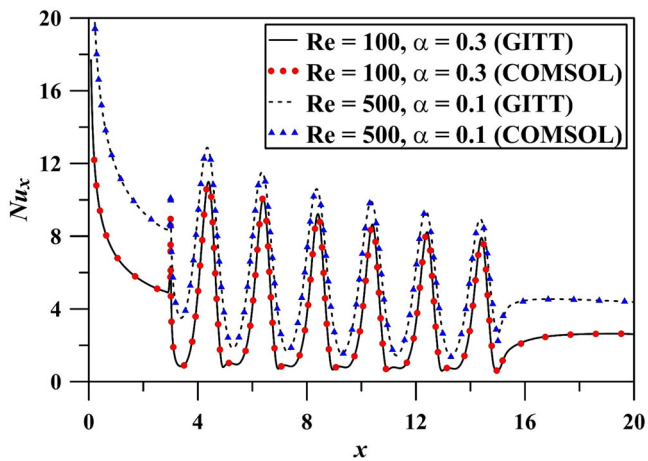
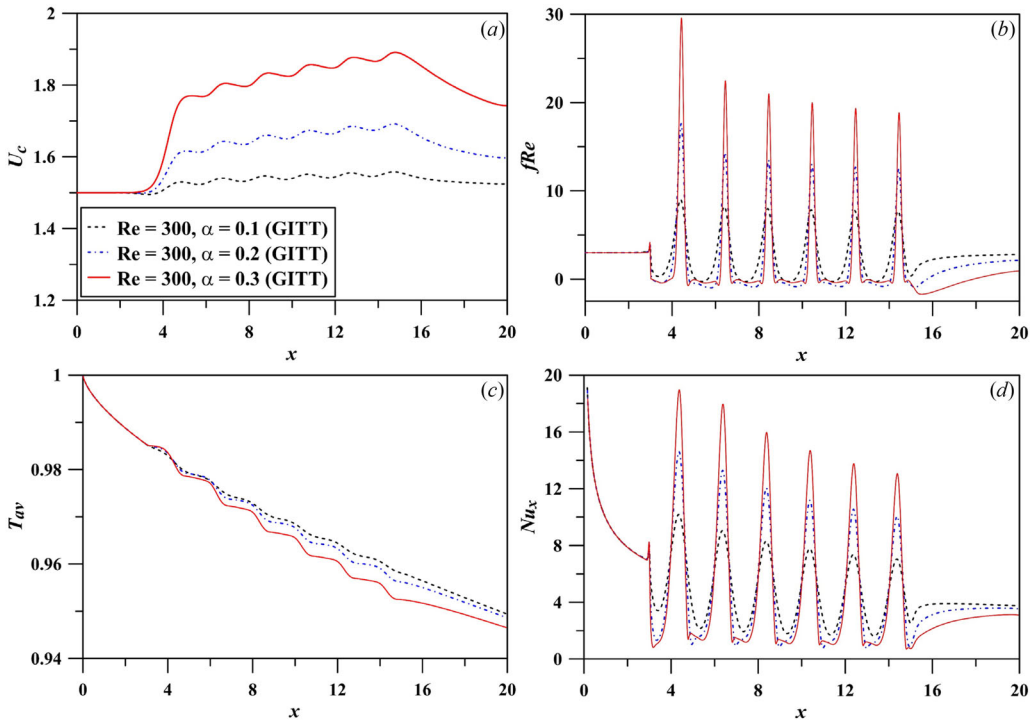


Figure 8. Comparisons of the local Nusselt number along the channel against COMSOL results.





**Figure 9.** Influence of the wave amplitude parameter for  $Re = 300$  on the (a) centerline longitudinal velocity component, (b)  $fRe$  product, (c) bulk temperature, and (d) local Nusselt number.

observe that the temperature convergence is achieved for four significant digits along all the wavy channel section with  $NV = NT = 50$  (even less terms in certain positions). For [Table 4](#), the convergence was achieved for  $NT = 70$ , which indicates that, as the Reynolds number is increased, the convergence is delayed at this wavy channel region.

The convergence for the friction factor and local Nusselt number are graphically demonstrated on [Figures 3](#) and [4](#), where one may observe that to graph scale the results are fully converged for truncation orders as low as  $NV = NT = 30$ . The results reconfirm the behavior observed in [Tables 3](#) and [4](#).

### 4.3. Results verification

[Figures 5–8](#) illustrate the results verification against an independent numerical solution for the axial velocity component at the channel centerline, bulk temperature,  $fRe$ , and local Nusselt number, respectively, along the longitudinal position. The comparisons are performed against the results obtained through COMSOL Multiphysics [\[42\]](#) (nonstructured mesh with maximum element size of  $5 \times 10^{-3}$ , boundary layer mesh with five layers, and error control of  $10^{-4}$ ). The cases considered are again  $Re = 100$  and  $\alpha = 0.3$ , and  $Re = 500$  and  $\alpha = 0.1$ . [Figure 5](#) shows the axial velocity component at the channel centerline, with good agreement between the GITT and COMSOL results. [Figure 6](#) also demonstrates the good agreement of the  $fRe$  obtained from the GITT and COMSOL results. Moreover, it is observed an overshoot at  $x = 3$  for both methods, which is caused by the domain transition from the regular flat section to the wavy plate at the beginning of the channel, which behaves like a sudden expansion. As can be observed in [Figure 6](#), the  $fRe$  product is constant at the parallel plates channel inlet and would present the same

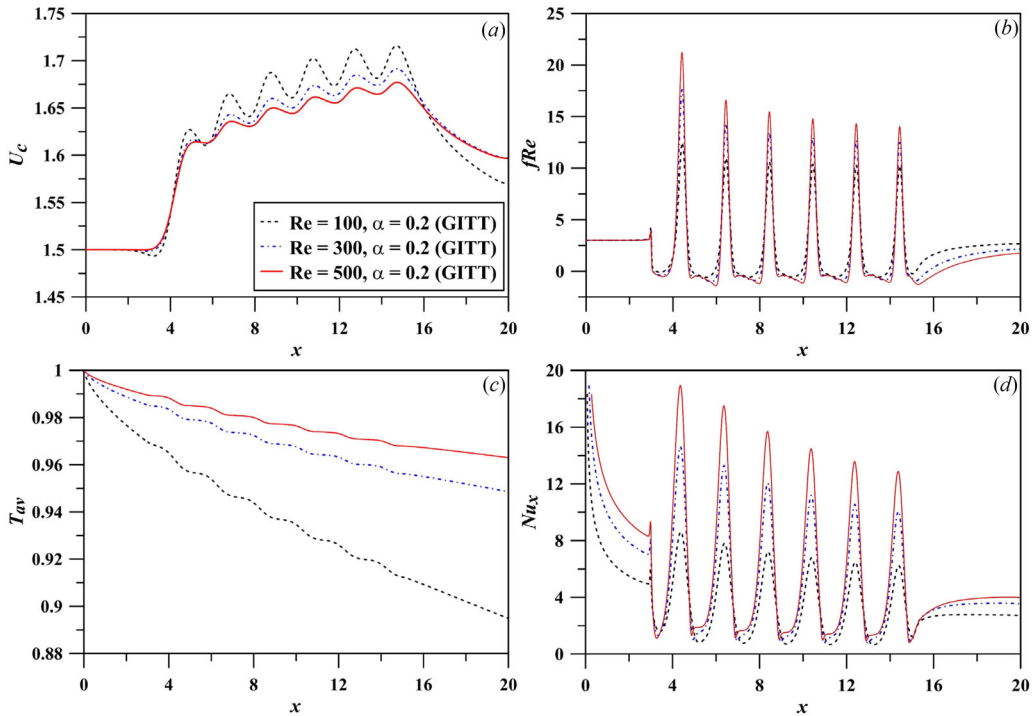


**Figure 10.** Influence of the Reynolds number for  $\alpha = 0.2$  on the (a) centerline longitudinal velocity component, (b)  $fRe$  product, (c) bulk temperature, and (d) local Nusselt number.

tendency at the outlet if it was extended enough once the flow reaches the fully developed region. It can be seen that when recirculation is present (especially for  $Re = 500$ ), the results are characterized by a sign change of the friction factor.

Figures 7 and 8 present the bulk temperature and the local Nusselt number,  $Nu_x$ , respectively, along the channel length. Again, the GITT results are in good agreement with the COMSOL computations. The same overshoot is observed at  $x = 3$  due to the sudden expansion effect at the domain abrupt transition.

#### 4.4. Effect of the wave amplitude

The wave amplitude effect was analyzed for  $Re = 300$  and  $\alpha = 0.1, 0.2$ , and  $0.3$ . Figures 9(a)–9(d) show the amplitude parameter influence on the centerline longitudinal velocity component and bulk temperature distributions, as well as on the  $fRe$  and local Nusselt number.

As can be observed, the increase in the wave amplitude, leads to an increase in the centerline velocity value (Figure 9(a)) and in the  $fRe$  product (Figure 9(b)). The recirculation zones again can be identified by the sign changes in the friction factor, at the axial positions where the boundary layer separation and reattachment occur. In this configuration, the vortex formation is noticeable in all the three cases, although, when  $\alpha = 0.1$ , the vortex is absent from the first period of the sinusoidal wave. The bulk temperature decreases with the increase in the wave amplitude (Figure 9(c)), due to a more effective heat transfer with the increased recirculation and heat exchange area, while the local Nusselt number is markedly increased from  $\alpha = 0.1$  to  $\alpha = 0.3$ , reconfirming the significant influence of the channel geometry on the heat transfer coefficient augmentation.

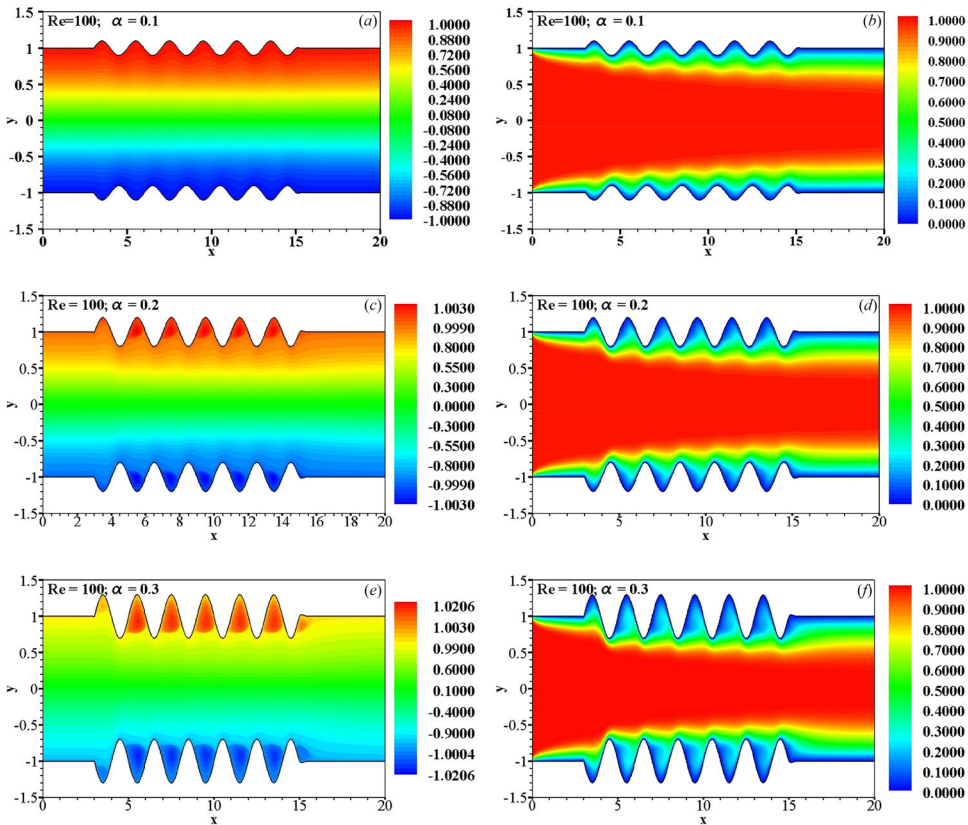


**Figure 11.** Streamfunction and temperature fields for  $Re=100$ : (a) streamfunctions for  $\alpha=0.1$ ; (b) temperatures for  $\alpha=0.1$ ; (c) streamfunctions for  $\alpha=0.2$ ; (d) temperatures for  $\alpha=0.2$ ; (e) streamfunctions for  $\alpha=0.3$ ; (f) temperatures for  $\alpha=0.3$ .

#### 4.5. Effect of the Reynolds number

The Reynolds number effect was analyzed for  $\alpha=0.2$  and  $Re = 100, 300,$  and  $500$ . Figures 10(a)–10(d) show the Reynolds number influence on the centerline longitudinal velocity component, bulk temperature, skin friction factor and Reynolds number product, and local Nusselt number.

It can be observed that the dimensionless centerline velocity values decrease from  $Re = 100$  to  $500$  (Figure 10(a)), even though the inertial forces are increased, due to the presence of more significant reverse flow and vortex zones. From the diminished amplitude of the longitudinal oscillations of the centerline velocity as  $Re$  increases, it can be said that the central flow is less disturbed by the channel corrugations, as can be observed in the bulk temperature behavior as well (Figure 10(c)). From Figures 10(b, d), it is also possible to observe that the  $fRe$  and the local Nusselt number have maximum values at the first period of the wave, which are progressively decreased along the channel. The minimum  $Nu_x$  value is reached right before the beginning of each wave, while its maximum values occur right before the wave crests.

#### 4.6. Streamfunction and temperature fields

Figures 11–13 present the dimensionless streamfunction and temperature fields for different values of the Reynolds number,  $Re=100, 300,$  and  $500$ , respectively, and of the wave amplitude

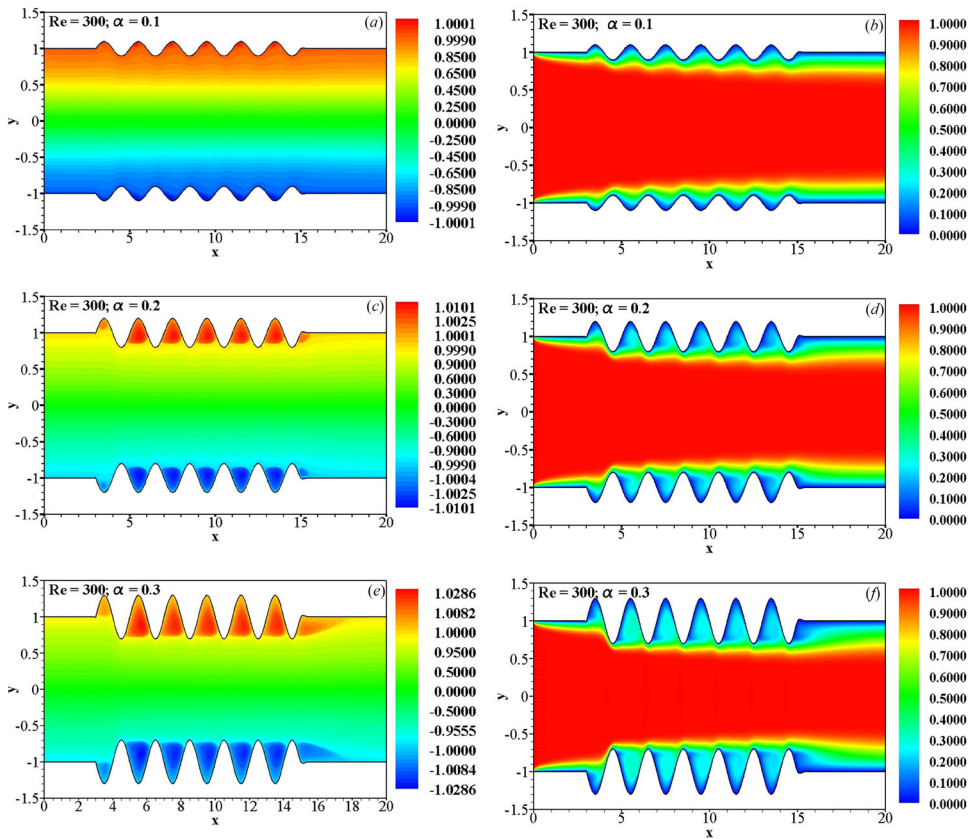


**Figure 12.** Streamfunction and temperature fields for  $Re=300$ : (a) streamfunctions for  $\alpha=0.1$ ; (b) temperatures for  $\alpha=0.1$ ; (c) streamfunctions for  $\alpha=0.2$ ; (d) temperatures for  $\alpha=0.2$ ; (e) streamfunctions for  $\alpha=0.3$ ; (f) temperatures for  $\alpha=0.3$ .

parameter ( $\alpha=0.1, 0.2$ , and  $0.3$ ). The dimensionless temperature values range from 0 to 1, with the inlet temperature value being 1 while the value at the walls is prescribed to 0. It can be observed the influence of the Reynolds number on the development of the velocity and temperature fields. For  $Re=100$ , the case with  $\alpha=0.1$  presented no recirculation zones (Figure 11(a)) and the boundary layer is always attached to the wall, resulting in lower heat transfer coefficients. As the wave amplitude is increased, with more pronounced recirculation zones, the thermal presence of the wall is sensed by the flow further into the channel cross section, as can be observed from the temperature fields in Figures 11. For  $Re=300$ , with  $\alpha=0.1$  (Figure 12(a)), the first vortex is formed already at the second wave. Again, as the wave amplitude is increased, the dimensionless temperature values decrease across the channel, indicating an increased heat transfer rate to the wall, more noticeably for the case  $\alpha=0.3$ . As the Reynolds number and the wave amplitude are increased, the recirculation zone occupies most of the wavy area, and a secondary vortex formation may even be observed for  $Re=300$  and  $\alpha=0.3$  (Figure 12(e)).

As the Reynolds number increases for a fixed wave amplitude, the heat transfer is increased as demonstrated by the increased Nusselt numbers (Figures 9(d) and 10(d)), but also by the wider more markedly thermally affected region into the channel cross section. It is also possible to observe the same behavior when the wave amplitude is increased, for a fixed Reynolds number (Figures 11–13), with increased heat transfer rates.

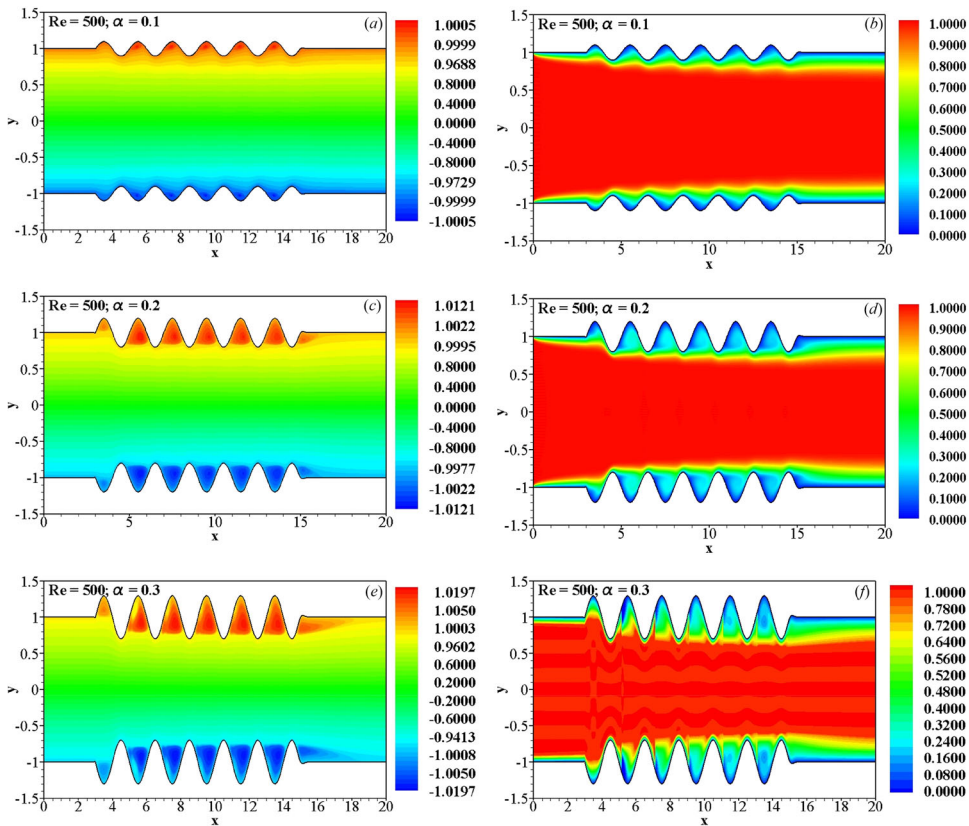


**Figure 13.** Streamfunction and temperature fields for  $Re=500$ : (a) streamfunctions for  $\alpha=0.1$ ; (b) temperatures for  $\alpha=0.1$ ; (c) streamfunctions for  $\alpha=0.2$ ; (d) temperatures for  $\alpha=0.2$ ; (e) streamfunctions for  $\alpha=0.3$ ; (f) temperatures for  $\alpha=0.3$ .

## 5. Conclusions

Heat and fluid flow in a wavy walls channel for a Newtonian fluid and incompressible laminar flow was analyzed, mathematically modeled by the steady state two-dimensional Navier–Stokes and energy equations and adopting the streamfunction-only formulation. The GITT hybrid numerical-analytical approach was successfully applied to the problem solution and the eigenfunction expansions convergence behavior was illustrated for the streamfunction field, skin friction coefficient, temperature field, and local Nusselt number along the channel. The results verification was performed by comparison against COMSOL v5.2 numerical results, with overall excellent agreement. Additional results were also presented for relevant quantities, toward a physical understanding and quantification of the heat transfer enhancement effect. The proposed model and the formal solution are sufficiently general to handle different boundary and inlet conditions, asymmetric configurations, and arbitrary geometrical forms, such as arc type or triangular wavy channels.

## Disclosure statement

No potential conflict of interest was reported by the authors.

## ORCID

Helder K. Miyagawa  <http://orcid.org/0000-0001-9346-4696>

João N. N. Quaresma  <http://orcid.org/0000-0001-9365-7498>

## References

- [1] T. Nishimura, S. Murakami, S. Arakawa, and Y. Kawamura, "Flow observations and mass transfer characteristics in symmetrical wavy-walled channels at moderate Reynolds numbers for steady flow," *Int. J. Heat Mass Transf.*, vol. 33, pp. 835–845, 1990. DOI: [10.1016/0017-9310\(90\)90067-5](https://doi.org/10.1016/0017-9310(90)90067-5).
- [2] T. A. Rush, T. A. Newell, and A. M. Jacobi, "An experimental study of flow and heat transfer in sinusoidal wavy passages," *Int. J. Heat Mass Transf.*, vol. 42, no. 9, pp. 1541–1553, 1999. DOI: [10.1016/S0017-9310\(98\)00264-6](https://doi.org/10.1016/S0017-9310(98)00264-6).
- [3] G. Wang and S. P. Vanka, "Convective heat transfer in periodic wavy passages," *Int. J. Heat Mass Transf.*, vol. 38, no. 17, pp. 3219–3230, 1995. DOI: [10.1016/0017-9310\(95\)00051-A](https://doi.org/10.1016/0017-9310(95)00051-A).
- [4] S. Pati, S. K. Mehta, and A. Borah, "Numerical investigation of thermo-hydraulic transport characteristics in wavy channels: comparison between raccoon and serpentine channels," *Int. Commun. Heat Mass Transf.*, vol. 88, pp. 171–176, 2017. DOI: [10.1016/j.icheatmasstransfer.2017.09.001](https://doi.org/10.1016/j.icheatmasstransfer.2017.09.001).
- [5] C. C. Wang and C. K. Chen, "Forced convection in wavy-wall channel," *Int. J. Heat Mass Transf.*, vol. 45, no. 12, pp. 2587–2595, 2002. DOI: [10.1016/S0017-9310\(01\)00335-0](https://doi.org/10.1016/S0017-9310(01)00335-0).
- [6] A. G. Ramgadia and A. K. Saha, "Numerical study of fully developed unsteady flow and heat transfer in asymmetric wavy channels," *Int. J. Heat Mass Transf.*, vol. 102, pp. 98–112, 2016. DOI: [10.1016/j.ijheatmasstransfer.2016.05.131](https://doi.org/10.1016/j.ijheatmasstransfer.2016.05.131).
- [7] A. G. Ramgadia and A. K. Saha, "Fully developed flow and heat transfer characteristics in a wavy passage: effect of amplitude of waviness and Reynolds number," *Int. J. Heat Mass Transf.*, vol. 55, no. 9–10, pp. 2494–2509, 2012. DOI: [10.1016/j.ijheatmasstransfer.2012.01.010](https://doi.org/10.1016/j.ijheatmasstransfer.2012.01.010).
- [8] A. G. Ramgadia and A. K. Saha, "Numerical study of fully developed flow and heat transfer in a wavy passage," *Int. J. Therm. Sci.*, vol. 67, pp. 152–166, 2013. DOI: [10.1016/j.ijthermalsci.2012.12.005](https://doi.org/10.1016/j.ijthermalsci.2012.12.005).
- [9] K. M. Lisboa *et al.*, "Mass transport enhancement in redox flow batteries with corrugated fluidic networks," *J. Power Sources*, vol. 359, pp. 322–331, 2017. DOI: [10.1016/j.jpowsour.2017.05.038](https://doi.org/10.1016/j.jpowsour.2017.05.038).
- [10] K. M. Lisboa and R. M. Cotta, "Analysis of the mass transport in corrugated membraneless flow batteries," *Appl. Math. Model.*, vol. 77, pp. 1512–1530, 2020. DOI: [10.1016/j.apm.2019.09.001](https://doi.org/10.1016/j.apm.2019.09.001).
- [11] H. M. S. Bahaidarah, N. K. Anand, and H. C. Chen, "Numerical study of heat and momentum transfer in channels with wavy walls," *Numer. Heat Transf., A Appl.*, vol. 47, no. 5, pp. 417–439, 2005. DOI: [10.1080/10407780590891218](https://doi.org/10.1080/10407780590891218).
- [12] H. M. S. Bahaidarah, "A numerical study of fluid flow and heat transfer characteristics in channels with staggered wavy walls," *Numer. Heat Transf. A Appl.*, vol. 51, no. 9, pp. 877–898, 2007. DOI: [10.1080/10407780600939644](https://doi.org/10.1080/10407780600939644).
- [13] M. A. Ahmed, M. Z. Yusoff, and N. H. Shuaib, "Effects of geometrical parameters on the flow and heat transfer characteristics in trapezoidal-corrugated channel using nanofluid," *Int. Commun. Heat Mass Transf.*, vol. 42, pp. 69–74, 2013. DOI: [10.1016/j.icheatmasstransfer.2012.12.012](https://doi.org/10.1016/j.icheatmasstransfer.2012.12.012).
- [14] P. M. M. Krishna, M. Deepu, and S. R. Shine, "Numerical investigation of wavy microchannels with rectangular cross section," *J. Enhanc. Heat Transf.*, vol. 25, no. 4–5, pp. 293–313, 2018. DOI: [10.1615/JEnhHeatTransf.2018021403](https://doi.org/10.1615/JEnhHeatTransf.2018021403).
- [15] Y. Sui, C. J. Teo, P. S. Lee, Y. T. Chew, and C. Shu, "Fluid flow and heat transfer in wavy microchannels," *Int. J. Heat Mass Transf.*, vol. 53, no. 13–14, pp. 2760–2772, 2010. DOI: [10.1016/j.ijheatmasstransfer.2010.02.022](https://doi.org/10.1016/j.ijheatmasstransfer.2010.02.022).
- [16] P. Mayeli, H. Hesami, and M. H. D. F. Moghaddam, "Numerical investigation of the MHD forced convection and entropy generation in a straight duct with sinusoidal walls containing water-Al<sub>2</sub>O<sub>3</sub> nanofluid," *Numer. Heat Transf. A Appl.*, vol. 71, no. 12, pp. 1235–1250, 2017. DOI: [10.1080/10407782.2017.1346998](https://doi.org/10.1080/10407782.2017.1346998).
- [17] A. Albojamal, H. Hamzah, A. Haghighi, and K. Vafai, "Analysis of nanofluid transport through a wavy channel," *Numer. Heat Transf. A Appl.*, vol. 72, no. 12, pp. 869–890, 2017. DOI: [10.1080/10407782.2017.1412679](https://doi.org/10.1080/10407782.2017.1412679).
- [18] A. Kumar, S. Nath, and D. Bhanja, "Effect of nanofluid on thermo hydraulic performance of double layer tapered microchannel heat sink used for electronic chip cooling," *Numer. Heat Transf. A Appl.*, vol. 73, no. 7, pp. 429–445, 2018. DOI: [10.1080/10407782.2018.1448611](https://doi.org/10.1080/10407782.2018.1448611).
- [19] P. Mayeli, H. Hesami, H. Besharati-Foumani, and M. Niajalili, "Al<sub>2</sub>O<sub>3</sub>-Water nanofluid heat transfer and entropy generation in a ribbed channel with wavy wall in the presence of magnetic field," *Numer. Heat Transf. A Appl.*, vol. 73, no. 9, pp. 604–623, 2018. DOI: [10.1080/10407782.2018.1461494](https://doi.org/10.1080/10407782.2018.1461494).

- [20] A. T. Al-Sammarraie, M. Al-Jethelah, M. R. Salimpour, and K. Vafai, "Nanofluids transport through a novel concave/convex convergent pipe," *Numer. Heat Transf. A Appl.*, vol. 75, no. 2, pp. 91–109, 2019. DOI: [10.1080/10407782.2019.1579517](https://doi.org/10.1080/10407782.2019.1579517).
- [21] M. Hatami, A. Kheirkhah, H. Ghanbari-rad, and D. Jing, "Numerical heat transfer enhancement using different nanofluids flow through venturi and wavy tubes," *Case Stud. Therm. Eng.*, vol. 13, pp. 1–10, 2019. DOI: [10.1016/j.csite.2018.100368](https://doi.org/10.1016/j.csite.2018.100368).
- [22] Y. T. Yang, H. W. Tang, and S. J. Jian, "Numerical simulation and optimization of turbulent nanofluids in a three-dimensional wavy channel," *Numer. Heat Transf. A Appl.*, vol. 69, no. 10, pp. 1169–1185, 2016. DOI: [10.1080/10407782.2015.1125729](https://doi.org/10.1080/10407782.2015.1125729).
- [23] Y. T. Yang, H. W. Tang, B. Y. Zeng, and M. H. Jian, "Numerical simulation and optimization of turbulent nanofluids in a three-dimensional arc rib-grooved channel," *Numer. Heat Transf. A Appl.*, vol. 70, no. 8, pp. 831–846, 2016. DOI: [10.1080/10407782.2016.1214513](https://doi.org/10.1080/10407782.2016.1214513).
- [24] M. Dehghani, "Entropy generation analysis of nanofluid forced convection in MHD plane diffuser," *Numer. Heat Transf. A Appl.*, vol. 75, no. 9, pp. 627–645, 2019. DOI: [10.1080/10407782.2019.1608772](https://doi.org/10.1080/10407782.2019.1608772).
- [25] R. M. Cotta, *Integral Transforms in Computational Heat and Fluid Flow*. Boca Raton, FL, USA: CRC Press, 1993.
- [26] R. M. Cotta and M. D. Mikhailov, "Hybrid methods and symbolic computations," in *Handbook of Numerical Heat Transfer*, 2nd ed., Chap. 16, W. J. Minkowycz, E. M. Sparrow, and J. Y. Murthy, Eds. New York, NY, USA: Wiley, 2006, pp.493–522.
- [27] R. M. Cotta *et al.*, "Analytical methods in heat transfer," in *Handbook of Thermal Science and Engineering*, Chap. 1, F. A. Kulacki, Eds. Switzerland: Springer International Publishing, 2018. DOI: [10.1007/978-3-319-32003-8\\_2-1](https://doi.org/10.1007/978-3-319-32003-8_2-1).
- [28] J. S. Pérez Guerrero and R. M. Cotta, "Lid-driven cavity flow problem in streamfunction-only formulation," *Int. J. Numer. Methods Fluids*, vol. 15, no. 4, pp. 399–409, 1992. DOI: [10.1002/fld.1650150403](https://doi.org/10.1002/fld.1650150403).
- [29] J. S. Pérez Guerrero and R. M. Cotta, "Integral transform solution of developing laminar duct flow in Navier-Stokes formulation," *Int. J. Numer. Methods Fluids*, vol. 20, no. 11, pp. 1203–1213, 1995. DOI: [10.1002/fld.1650201102](https://doi.org/10.1002/fld.1650201102).
- [30] J. S. Pérez Guerrero, J. N. N. Quaresma, and R. M. Cotta, "Simulation of laminar flow inside ducts of irregular geometry using integral transforms," *Comput. Mech.*, vol. 25, no. 4, pp. 413–420, 2000. DOI: [10.1007/s004660050488](https://doi.org/10.1007/s004660050488).
- [31] F. A. Pontes, E. N. Macêdo, C. da, S. Batista, J. A. de Lima, and J. N. N. Quaresma, "Hybrid solutions obtained via integral transforms for magnetohydrodynamic flow with heat transfer in parallel-plate channels," *Int. J. Numer. Methods Heat Fluid Flow*, vol. 28, no. 7, pp. 1474–1505, 2018. DOI: [10.1108/HFF-02-2017-0076](https://doi.org/10.1108/HFF-02-2017-0076).
- [32] K. M. Lisboa and R. M. Cotta, "Hybrid integral transforms for flow development in ducts partially filled with porous media," *Proc. R. Soc. A*, vol. 474, no. 2209, pp. 20170637, 2018. DOI: [10.1098/rspa.2017.0637](https://doi.org/10.1098/rspa.2017.0637).
- [33] K. M. Lisboa and R. M. Cotta, "On the mass transport in membraneless flow batteries with flow-by configuration," *Int. J. Heat Mass Transf.*, vol. 122, pp. 954–966, 2018. DOI: [10.1016/j.ijheatmasstransfer.2018.02.002](https://doi.org/10.1016/j.ijheatmasstransfer.2018.02.002).
- [34] K. M. Lisboa, J. Su, and R. M. Cotta, "Single domain integral transform analysis of natural convection in cavities partially filled with heat generating porous medium," *Numer. Heat Transf. A Appl.*, vol. 74, no. 3, pp. 1068–1086, 2018. DOI: [10.1080/10407782.2018.1511141](https://doi.org/10.1080/10407782.2018.1511141).
- [35] K. M. Lisboa, J. Su, and R. M. Cotta, "Vector eigenfunction expansion in the integral transform solution of transient natural convection," *Int. J. Numer. Methods Heat Fluid Flow*, vol. 29, no. 8, pp. 2684–2708, 2019. DOI: [10.1108/HFF-10-2018-0543](https://doi.org/10.1108/HFF-10-2018-0543).
- [36] R. M. Cotta *et al.*, "A review of hybrid integral transform solutions in fluid flow problems with heat or mass transfer and under Navier-Stokes equations formulations," *Numer. Heat Transf. B Fundam.*, vol. 76, no. 2, pp. 60–87, 2019. DOI: [10.1080/10407790.2019.1642715](https://doi.org/10.1080/10407790.2019.1642715).
- [37] R. L. Silva, J. N. N. Quaresma, C. A. C. Santos, and R. M. Cotta, "Integral transforms solution for flow development in wavy wall ducts," *Int. J. Numer. Methods Heat Fluid Flow*, vol. 21, pp. 219–243, 2010. DOI: [10.1108/09615531111105416](https://doi.org/10.1108/09615531111105416).
- [38] F. V. Castellões, J. N. N. Quaresma, and R. M. Cotta, "Convective heat transfer enhancement in low Reynolds number flows with wavy walls," *Int. J. Heat Mass Transf.*, vol. 53, no. 9–10, pp. 2022–2034, 2010. DOI: [10.1016/j.ijheatmasstransfer.2009.12.054](https://doi.org/10.1016/j.ijheatmasstransfer.2009.12.054).
- [39] R. M. Cotta *et al.*, "Recent advances in computational-analytical integral transforms for convection-diffusion problems," *Heat Mass Transf.*, vol. 54, no. 8, pp. 2475–2496, 2018. DOI: [10.1007/s00231-017-2186-1](https://doi.org/10.1007/s00231-017-2186-1).
- [40] IMSL® Fortran Numerical Library, Version 2018. Boulder, CO, USA: Rogue Wave Software Inc., 2018.
- [41] S. Wolfram, *Mathematica v.11*. Champaign, IL: Wolfram Research Inc., 2018.
- [42] COMSOL Multiphysics® v. 5.2, Stockholm, Sweden: COMSOL AB, 2015.